

Technical electrodes catalyzed with PtRu on mesoporous ordered carbons for liquid direct methanol fuel cells

Garbiñe Álvarez · Francisco Alcaide · Oscar Miguel · Laura Calvillo ·
María Jesús Lázaro · Jacob J. Quintana · Juan Carlos Calderón · Elena Pastor

Received: 12 May 2009 / Revised: 29 July 2009 / Accepted: 31 July 2009 / Published online: 13 August 2009
© Springer-Verlag 2009

Abstract This paper presents the behavior of ordered mesoporous carbon (OMC)-supported catalysts as anodes for direct methanol fuel cells (DMFC), fed with an aqueous methanol solution. OMC samples were prepared by the nanocasting method from a polymerized furan resin using mesoporous silica as a template. Pt and PtRu nanoparticles were supported on OMC with high dispersion, the particle size being 2.4 nm at PtRu loading of 15 wt.%. The resulting catalysts were analyzed using carbon monoxide stripping voltammetry, cyclic voltammetry, and chronoamperometry in three-electrode experiments and recording cell voltage vs. current density curves in practical DMFC. It was found that PtRu-catalyzed technical electrodes exhibited good activity towards methanol electrooxidation in half-cell experiments under fuel-cell-relevant conditions. Specifically, Pt₈₅Ru₁₅/OMC catalyst showed the highest catalytic enhancement compared to Pt/OMC for the steady-state electrooxidation of methanol at 60 °C and 0.5 V, by a factor of 22 in 2-M MeOH solution. DMFC single cells yielded an open-circuit voltage of 0.625 V at 60 °C. Polarization curves indicate that DMFC with OMC-

supported Pt₈₅Ru₁₅ catalyst at the anode exhibited the best performance.

Keywords Methanol electrooxidation · Direct methanol fuel cell · DMFC · PtRu catalyst · Ordered mesoporous carbon

Introduction

Direct liquid methanol fuel cells (*liquid*-DMFC) are promising energy sources for mobile and portable applications, mainly because of the methanol advantages against hydrogen, such as its higher solubility in liquid electrolytes, availability at low cost, and easier handling, transport, and storage. In addition, methanol has a high energy density (6 kWh kg⁻¹) [1]. From a practical perspective, there is a wide range of devices covering several operational conditions. For example, cell phones and PDAs (small power devices) will operate at 40 °C or lower, whereas laptops, power tools, and battery chargers for army or remote site applications (intermediate power devices) will operate at 60–80 °C [2]. However, the commercial use of DMFC is still limited due to high costs and insufficient durability [3]. Recently, considerable effort has been directed towards the development of high catalytic activity electrodes for methanol oxidation at low Pt content. This optimization of the electrocatalyst basically involves two routes: (1) the development of new catalyst syntheses with attention to alloy composition, nanometric dimensions, and uniform distribution of the catalyst on the carbon support and (2) the development of new carbon supports of high electric conductivity and elevated mesoporosity in the pore size range of 20–40 nm for a high accessible surface area.

Traditionally, the improvement of the catalyst supports has received less attention. Meanwhile, structural character-

G. Álvarez · F. Alcaide (✉) · O. Miguel
Departamento de Energía, CIDETEC,
Pº Miramón, 196,
20009 Donostia/San Sebastián, Spain
e-mail: falcaide@cidetec.es

L. Calvillo · M. J. Lázaro
Instituto de Carboquímica, CSIC,
Miguel Luesma Castán 4,
50018 Zaragoza, Spain

J. J. Quintana · J. C. Calderón · E. Pastor
Departamento de Química Física, Universidad de La Laguna,
Avda. Astrofísico Francisco Sánchez s/n,
38071 San Cristóbal de La Laguna, Santa Cruz de Tenerife, Spain

istics of carbon materials, like porosity, specific surface area, and surface properties, among others, exert a strong influence on the fuel cell performance, through aspects like the size and morphology of metal nanoparticles, catalyst stability, metal/ionomer contact and catalyst utilization, mass transport, and water management. Because of this, many research groups have recently made efforts to use various novel carbon supports such as nanotubes, nanofibers, and mesoporous carbons for fuel cell applications [4]. The presence of nanopores (≤ 2 -nm diameter) in these carbon supports leads to a poor utilization of the catalysts since the catalyst particles inside the micropores are inaccessible to the fuel. Then, to enhance both the dispersion and utilization of the catalysts, carbons with high surface area, large pore diameter, and high pore volume are needed. In this regard, ordered mesoporous carbons (OMC) with pore diameters from 2 to 50 nm are attractive as they possess a combination of high surface area and large pore diameter, while microporous carbons with much larger pore diameters (≥ 50 nm) may experience a decrease in surface area [5].

The preparation of OMC as a platinum support for their use in polymer electrolyte membrane fuel cell cathodes has been reported in the literature [6, 7]. On the other hand, anodic methanol oxidation has not been studied on Pt/OMC. The Pt-loaded mesoporous carbon samples with controlled porosity exhibit two to three times higher mass activities than Pt/Vulcan XC-72R for methanol electro-oxidation [8, 9]. About this, it has been shown that colloidal methods for preparing highly dispersed Pt on mesoporous carbon supports yield catalysts more active towards the methanol oxidation reaction than those prepared by impregnation methods [10]. Other methods, like those based on the pyrolysis of carbon and Pt precursors in mesoporous silica, have given good results in terms of size, shape, and dispersion, as well as activity towards methanol oxidation [11]. In addition, DMFC single-cell tests showed that Pt/OMC used as cathode catalyst exhibited higher performance than the commercial catalyst [12].

Many accept that PtRu is the best catalyst for methanol oxidation because of its high tolerance for CO poisoning. However, there is much discussion on the effect of the Ru content. In the literature, we can find contradictory results, but in general the best Pt-to-Ru atomic ratio for anodic methanol oxidation varies from 10% at room temperature to 50% at 60 °C [13].

Half-cell studies with PtRu over mesoporous carbons indicate a high activity of this catalyst towards methanol oxidation [14–20] and their ability to be used in practical DMFC anodes. Other kinds of carbon supports with a developed mesoporous structure, like spherical carbon capsules with hollow macroporous core and mesoporous shell structures [21], as well as aerogels [22], have

demonstrated their suitability as a support of PtRu catalysts for anodes in DMFC. Pt–Cr supported on mesoporous carbon has also been used as catalyst for anodes in DMFC [23]. Nevertheless, limited attention has been given to the study of the electrochemical behavior of PtRu/OMC as an anode catalyst in practical DMFCs.

In this paper, we report the electrochemical behavior of PtRu nanoparticles supported on OMC towards methanol electrooxidation in half-cell and single DMFC, under operating conditions used in practical fuel cells, in addition to their suitability for their use as anodic electrocatalysts in these fuel cell systems.

Experimental

Preparation of carbon support

OMC were prepared by the nanocasting method, as previously described [24]. Briefly, the method consisted of the incipient wetness impregnation of ordered mesoporous silica (SBA-15) with a mixture of polymerized furan resin (Hüttenes Albertus) and acetone (resin-to-acetone mass ratio=5). Impregnated silica was cured at 108 °C for 24 h and carbonized at 700 °C for 3 h. Subsequently, the resulting silica–carbon composite was stirred in a hydrogen fluoride aqueous solution for 24 h to remove the silica. Carbon materials were washed carefully with distilled water until the pH of the filtrate reached 7. Finally, carbon materials were dried at 108 °C. They had a specific area of 570 m² g⁻¹ and a pore volume of 0.37 cm³ g⁻¹ and were designated as CMK-3.

CMK-3 carbon was refluxed in diluted (2 mol dm⁻³) or concentrated (65 wt.%) HNO₃ solutions to create surface oxygen groups. These oxidation treatments were carried out at room temperature for 0.5 or 2 h. Finally, oxidized CMK-3 carbons were filtered, washed exhaustively with distilled water, and dried at 108 °C.

Synthesis of catalysts and structural characterization

PtRu electrocatalysts supported on OMC and Vulcan XC-72 (Cabot Corp.) were prepared by the formic acid method (FAM) [25]. Briefly, the procedure was as follows: first, the formic acid solution was added to the carbon material at 80 °C. Then, metal precursor (H₂PtCl₆ 6H₂O and RuCl₃, both Alfa Aesar) solution was slowly dropped under sonication to obtain a good dispersion of the PtRu/OMC. The atomic ratio of Pt to Ru and the metal loading-to-carbon ratio were adjusted using appropriate concentrations of Pt and Ru in solution. A similar procedure was used to prepare Pt/OMC but using NaBH₄ as a reducing agent [26].

Structural characterization of the catalysts was done by the X-ray diffraction (XRD) technique. XRD spectra were collected using a universal diffractometer Carl Zeiss-Jena, URD-6, with CuK_α radiation and a 2θ scan from 0° to 100° (at 3° min^{-1}). To estimate the particle size of the dispersed metal crystallites, Scherrer's equation was used [27]:

$$D = k \lambda / B \cos \theta \quad (1)$$

where D is the mean particle size (\AA); k is a coefficient taken here as 0.9 [28]; λ is the wavelength of the X-rays used (1.5406 \AA); B is the width of the diffraction peak at half height (rad), and θ is the angle at the position of the peak maximum. To determine B , the (220) peak of the Pt face-centered cubic (fcc) structure around $2\theta=70^\circ$ was selected.

On the other hand, the lattice parameters were obtained by refining the unit cell dimensions by the least square method [29].

The mass ratio of PtRu to carbon in the electrocatalysts and Pt-to-Ru atomic ratios were analyzed by the energy-dispersive X-ray (EDX) technique. The EDX measurements were performed with an INCA-300 energy analyzer coupled to a scanning electron JSM5910-LV JEOL microscope.

Electrode preparation and electrochemical characterization

All technical electrodes used through this work were thin-film diffusion electrodes. They consist of a diffusion layer and a catalyst layer. The gas diffusion layer was ELAT[®] V2.1 (E-TEK, Inc.). To fabricate the catalyst layer, an ink was prepared by suspending the catalyst in water and agitating in an ultrasonic bath for 30 min to thoroughly wet and disperse the catalyst. Enough 5% Nafion[®] dispersion solution (Aldrich) was then added to the mixture to give a dry ink composition of 20wt.% Nafion[®] ionomer. The mixtures were subjected to ultrasound for another 2 h at room temperature to obtain uniformly dispersed inks. The catalyst inks were sprayed onto the gas diffusion layer by an air gun and dried at 70°C , until a catalyst loading of 2 mg cm^{-2} was achieved. The catalyst loading was determined gravimetrically, using an analytical balance STA-60/200 (Gram Precision) with a resolution of 0.01 mg.

The electrochemical measurements were conducted via a potentiostat PGSTAT 30 (Eco Chemie) driven by the GPES software in a thermostated three-compartment electrochemical glass cell. Potentials were measured using a $\text{Hg}|\text{Hg}_2\text{SO}_4, \text{K}_2\text{SO}_{4\text{sat}}$ reference electrode (MSE) separated from the working electrode compartment by a tube ended in a Luggin capillary. However, in this study, we have referred those to that of the reversible hydrogen electrode. The counter electrode consisted of a Pt wire separated from

the main solution by a fritted glass. Working electrodes of 0.79-cm^2 geometric area were mounted inside a holder. A gold mesh acted as a current collector. The design of the electrode holder allowed for a N_2 stream to pass around the back of the electrode.

Electrodes were immersed into the N_2 -purged electrolyte ($0.50 \text{ mol dm}^{-3} \text{ H}_2\text{SO}_4$, Merck Suprapure) and were cycled between 0.075 and 0.8 V, until the voltammogram was reproducible. The positive potential applied to PtRu-catalyzed electrodes was limited to 0.750 or 0.800 V in order to avoid Ru dissolution. For CO stripping voltammetry, CO (CO (1,000 ppm)/ N_2 , Praxair, 5.0) was adsorbed onto the electrode surface at 0.100 V for 30 min. Subsequently, the electrolyte was purged with N_2 for 20 min before the stripping peak was measured.

For methanol (MeOH) oxidation measurements, a N_2 -purged electrolyte of $2.0 \text{ mol dm}^{-3} \text{ MeOH} + 0.50 \text{ mol dm}^{-3} \text{ H}_2\text{SO}_4$ was used. Cyclic voltammetry was performed between 0.075 and 0.800 V. In chronoamperometric measurements, the electrodes were stepped to potentials between 0.400 and 0.550 V. At each potential, the electrodes were held for 30 min to simulate steady-state conditions. One data set was always recorded with a single electrode, that is, after stepping from 0.050 to 0.400 V, the next step to 0.450 V was performed with another electrode.

Preparation of the membrane electrode assembly

Membrane electrode assemblies (MEAs) with geometrical area of 5 cm^2 were prepared using the hot press method. Technical electrodes catalyzed with PtRu/OMC were used as anodes. Cathodes contained a commercially available 20 wt.% Pt/Vulcan XC-72R catalyst (E-Tek, Inc.) with a loading of $2.0 \text{ mg}_{\text{Pt}} \text{ cm}^{-2}$, which was kept identical for all the MEAs.

Nafion[®] 115 membranes were cleaned and converted into the acid form by boiling in 3% H_2O_2 for 1 h, following by boiling in 0.5 M H_2SO_4 for 2 h, and finally boiling in ultrapure water for 2 h with the water being changed every 30 min. The cleaned membrane was stored in ultrapure water and dried before use.

Each MEA was assembled by hot pressing the anode and cathode on either side of the pretreated membrane at 50 bar and 130°C for 180 s.

Operation of liquid-DMFC

The MEAs were mounted into a commercial 5-cm^2 cell hardware (Fuel Cell Technologies). The current collectors consisted of POCO graphite blocks (Poco Graphite, Inc.) with machined serpentine flow fields for the MeOH and O_2 feeds. The cell was held together between two gold-plated

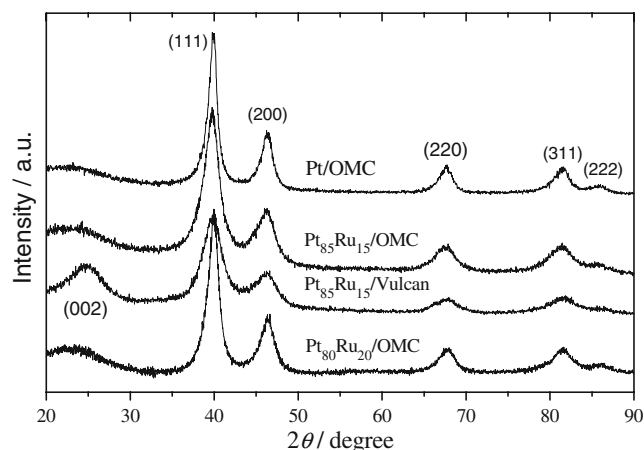


Fig. 1 X-ray diffraction patterns of supported Pt and PtRu catalyst

stainless steel contact plates using a set of retaining bolts positioned around the periphery of the cell. The cell contained also electrical heaters, a thermocouple, and voltage connectors. Polytetrafluoroethylene-reinforced gaskets were inserted to prevent the cell from leaking. Single cells were operated with a 2.0 mol dm^{-3} aqueous MeOH solution pumped through the anode compartment at 1.5 ml min^{-1} and zero back-pressure from a reservoir at $60 \text{ }^\circ\text{C}$, and with dry O_2 from cylinders passed through the cathode compartment at 50 standard cubic centimeters per minute and zero back-pressure.

The fuel cells were conditioned for 3 days before the polarization data were taken using the following procedure: the DMFC was heated to $60 \text{ }^\circ\text{C}$ at open circuit with methanol solution circulating through the anode and O_2 flowing through the cathode for 1 h. Then, the cell was operated at 40 mA cm^{-2} for 2 h. After that, the cell was operated at 0.400 V for another 2 h. The cell was then shut down by turning off the load, heating, MeOH, and O_2 supply and left overnight at room temperature. The performance of the DMFCs stabilized after such conditioning. Steady-state polarization curves were measured using a computer-controlled potentiostat 1287A (Solartron Analytical, Inc.) in the potentiodynamic polarization mode at a scan rate of 5 mV s^{-1} .

Results and discussion

Structural characterization of catalysts by XRD analysis

XRD patterns of Pt- and PtRu-supported catalysts are shown in Fig. 1. The broad peaks (002) in all diffractograms at about $2\theta=25^\circ$ are associated with the carbon support material. The different shapes of OMC and Vulcan support-assigned peaks indicate a higher surface area for the latter carbon support. The crystalline structure of the metal in the nanoparticles is evident, and all XRD patterns display the (111), (200), (220), (311), and (222) reflection characteristic of the fcc crystal structure of Pt. Reflections (100), (101), (110), (103), and (201) characteristic of the Ru hexagonal close-packed crystal structure are not observed. This result suggests that, for materials prepared in this work, Ru is incorporated in the Pt fcc structure. This is supported by the fact that diffraction peaks in PtRu-supported catalysts are slightly shifted to higher 2θ values with respect to the same reflection peaks in Pt catalyst, showing the effect of increasing amounts of Ru in the electrocatalysts and suggesting the formation of a PtRu alloy [30].

The lattice parameters were calculated from the XRD patterns in Fig. 1, considering the reflection peak position for Pt signals. The results are summarized in Table 1. The value for the $\text{Pt}_{80}\text{Ru}_{20}/\text{OMC}$ electrocatalyst (3.910 \AA) is lower than that of Pt/OMC (3.913 \AA), indicating a contraction of the lattice due to the PtRu alloying to some extent. This result agrees well with those reported by Chu and Gilman working with PtRu-unsupported alloy electrocatalysts, which found a decrease of the lattice parameter due to incorporation of Ru atoms in the fcc structure of Pt, and they showed that in all cases Ru was alloyed with Pt [30]. Thus, the decrease observed for the lattice parameter in the present work corroborates the formation of a PtRu alloy in the electrocatalyst. It is remarkable that the value of the lattice parameter for $\text{Pt}_{85}\text{Ru}_{15}/\text{OMC}$ catalyst does not match the previous arguments but, as shown in [31], follows the general behavior observed for the Pt materials prepared with FAM.

Table 1 Composition from EDX and physical parameters from XRD analysis of the Pt- and PtRu-supported catalysts

Catalyst	Pt/Ru ^a (at.%)	Metal loading (wt.%)	Mean particle size (nm)	Lattice parameter (\AA)	SA ^b (m^2g^{-1})
Pt/OMC	100:0	17	4.5	3.913	62
$\text{Pt}_{80}\text{Ru}_{20}/\text{OMC}$	80:20	10	4.3	3.910	68
$\text{Pt}_{85}\text{Ru}_{15}/\text{OMC}$	85:15	15	3.2	3.918	91
$\text{Pt}_{85}\text{Ru}_{15}/\text{Vulcan}$	85:15	17	2.9	3.913	100

^a Pt-to-Ru atomic ratio determined by EDX measurements

^b Metal surface area

On the other hand, particle size affects the lattice parameter. The dependence of the lattice parameter on the particle size for electrocatalysts prepared by the formic and borohydride method has been described previously [31–33]. It was observed that the increase in the particle size for OMC-supported electrocatalysts produces a diminution in the lattice parameter, an effect which is more apparent when the FAM is used [31]. Accordingly, the lattice parameter for Pt₈₅Ru₁₅/OMC (3.918 Å) is higher than that for Pt₈₅Ru₁₅/Vulcan (3.913 Å), as the particle size of former catalyst is 3.2 nm, whereas the latter is 2.9 nm for the same Pt/Ru atomic composition, that is, an expansion of the lattice of Pt occurs because of the increase in the particle size for these PtRu materials. Mean particle sizes for the electrocatalysts calculated by Eq. 1 are summarized in Table 1.

The metal surface areas (SA) were calculated by applying the equation:

$$SA = 6 \times 10^3 / \rho d \quad (2)$$

where SA is the surface area of metallic nanoparticles (m² g⁻¹); *d* is the mean particle size (nm), and ρ (g cm⁻³) is the density of Pt or PtRu alloys ($\rho = \rho_{\text{Pt}} X_{\text{Pt}} + \rho_{\text{Ru}} X_{\text{Ru}}$, where $\rho_{\text{Pt}} = 21.45$ g cm⁻³, $\rho_{\text{Ru}} = 12.45$ g cm⁻³, and X_{Pt} or X_{Ru} are the weight percent of Pt and Ru in the catalyst). The SAs calculated using Eq. 2 are shown in Table 1. The SAs increase with decrease in the particle size.

Table 1 also shows the atomic composition of Pt- and PtRu-supported electrocatalysts prepared in this work determined by EDX. The Pt and PtRu bulk compositions detailed here represent the average of five different measurements on the same sample. These values presented a standard relative error less than 1%.

CO stripping voltammetry

To determine the electrochemically active surface area of the catalyst particles and to obtain some information on their surface composition, we characterized them by CO stripping experiments [34]. The resulting stripping voltammograms are shown in Fig. 2. The curves were recorded at 20 °C for (c) the Pt₈₀Ru₂₀/OMC, (b) Pt₈₅Ru₁₅/OMC, and (a) Pt/OMC for comparison (Fig. 2a).

The stripping peak potential shown in Fig. 2a (a) for the Pt/OMC catalyst is 0.81 V. This value agrees well with that obtained on pure Pt or Pt/Vulcan (≈ 0.80 V) [35, 36], taking into account the error range mainly due to the variations in the potential measurement (± 10 mV). In addition, the stripping peak potentials of the PtRu/OMC Fig. 2a (b, c) catalysts are significantly lower than those obtained on Pt/OMC catalyst. Catalyst b shows a single CO oxidation peak centered at 0.65 V, whereas catalyst c shows two peaks centered at 0.58 and 0.50 V. This latter

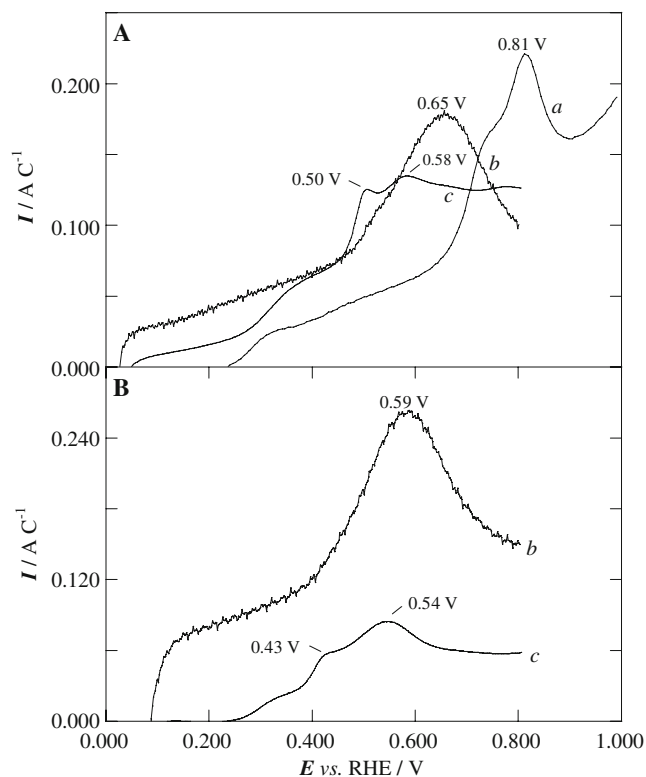


Fig. 2 CO stripping scans at **a** 20 °C and **(b)** 60 °C for anodes catalyzed with: **(a)** Pt/OMC, **(b)** Pt₈₅Ru₁₅/OMC, and **(c)** Pt₈₀Ru₂₀/OMC. H₂SO₄ 0.5 mol dm⁻³. $v = 20$ mV s⁻¹. The currents were normalized by the CO_{ads} charge to better compare the data

behavior suggests the existence of a nonhomogeneous alloy composition for this catalyst. However, PtRu/OMC catalysts exhibited an enhanced CO tolerance compared to Pt/OMC catalysts. Therefore, PtRu/OMC catalysts exhibited an enhanced CO tolerance compared to Pt/OMC catalysts. This behavior could be explained by a bifunctional mechanism according to the higher affinity of Ru for H₂O or OH species than that of Pt, with the result that CO adsorbed onto the electrode surface can be oxidized into CO₂ at lower potentials [37].

CO stripping experiments at room temperature have a limited validity for conclusions on the catalyst behavior under practical fuel cell operating conditions. Then, the electrochemical oxidation of CO at 60 °C was studied in a second series of experiments. The CO stripping voltammograms measured at 60 °C on PtRu/OMC-catalyzed electrodes are shown in Fig. 2b. The profiles for both catalysts are similar compared to the profiles at 20 °C. However, it seems that higher temperature could enhance the electrocatalytic activity of the PtRu/OMC catalysts towards oxidation of adsorbed CO because the CO oxidation peak potentials are shifted to less anodic potentials with respect to 20 °C. A similar behavior was reported for other PtRu-supported catalysts [38–40].

Potentiodynamic methanol oxidation

Cyclic voltammograms for methanol oxidation on Pt/OMC and PtRu/OMC electrodes were obtained after the electrode was immersed in the solution for 5 min by sweeping the potential negatively from the open-circuit potential and then up to 0.800 or 1.0 V. From Fig. 3, the onset of the methanol oxidation on Pt/OMC in the forward sweep of curve c (dotted line) can be estimated between 0.55 and 0.60 V, while MeOH oxidation current peaks are clearly observed at 0.86 and 0.82 V in the anodic and cathodic sweeps, respectively. Moreover, during the first positive going sweep, the oxidation of methanol on Pt₈₀Ru₂₀/OMC-catalyzed electrode starts at 0.500 V. The oxidation current increases considerably with increasing potential until 0.800 V (curve b). Upon reversing the scan at 0.800 V, no peak or hysteresis loop in the current response is observed. These facts suggest that there is virtually no accumulation of poisons on the electrode surface when the potential is more negative than 0.800 V over the timescale of the experiment [41]. In addition, cyclic voltammogram for Pt₈₅Ru₁₅/OMC-catalyzed (curve a) electrode shows a shift of the onset MeOH oxidation to a lower anodic potential (70 mV) compared to the former electrode and results in better catalyst activity towards methanol oxidation.

Potentiostatic methanol electrooxidation

To study the catalyst activity under “long-term” fuel-cell-relevant conditions, which is especially important when studying such self-poisoning reactions as methanol electrooxidation, we have carried out tests at constant potential. From a practical point of view, the catalytic

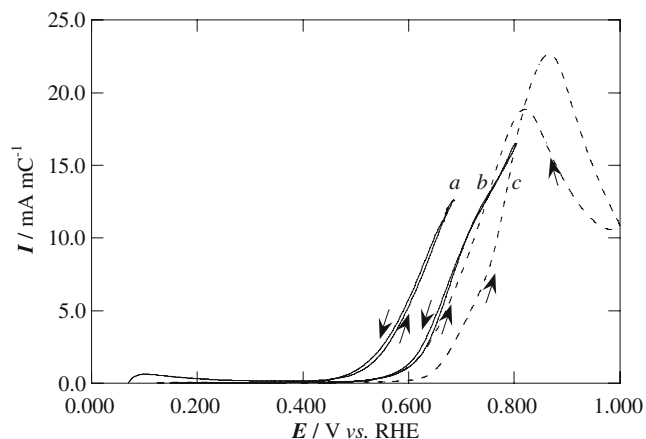


Fig. 3 Cyclic voltammograms for (a) Pt₈₅Ru₁₅/OMC-, (b) Pt₈₀Ru₂₀/OMC-, and (c) Pt/OMC-catalyzed technical electrodes in 0.5 mol dm⁻³ H₂SO₄ aqueous solution containing 2.0 mol dm⁻³ methanol at 60 °C. $v = 20$ mV s⁻¹. The currents were normalized by the CO_{ads} charge (determined at 20 °C) to better compare the data

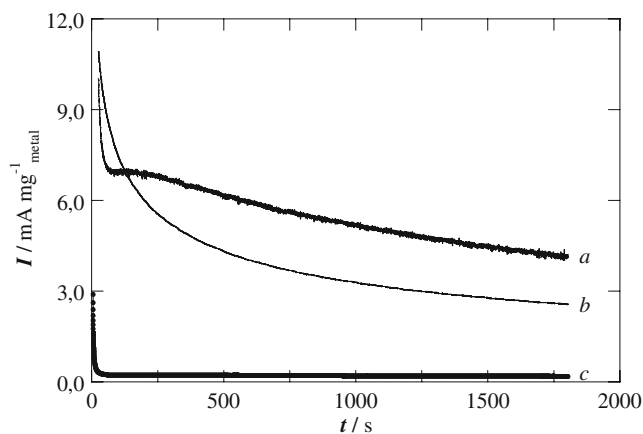


Fig. 4 Potentiostatic electrooxidation of methanol over (a) Pt₈₅Ru₁₅/OMC-, (b) Pt₈₀Ru₂₀/OMC-, and (c) Pt/OMC-catalyzed electrodes at 0.500 V. 0.50 mol dm⁻³ H₂SO₄+2.0 mol dm⁻³ MeOH. Temperature 60 °C. Currents were normalized by the total metal content in the electrodes

activity can be measured, expressing the resulting current per unit of catalyst mass [42]. Figure 4 shows the mass-specific current of methanol oxidation as a function of time at 0.500 V for the Pt/OMC and PtRu/OMC catalysts in H₂SO₄ 0.5-mol dm⁻³ aqueous solution containing methanol 2.0 mol dm⁻³ at 60 °C. The three curves feature a sharp decrease during the first minutes. Afterwards, the current diminishes much more slowly. This behavior has been reported earlier for methanol oxidation on Pt and PtRu catalysts. The loss of activity has been ascribed to catalyst poisoning by methanol dehydrogenation fragments and to the formation of Ru oxides and/or the presence of surface active impurities or anions in the electrolyte solution that may slowly adsorb onto the catalyst surface [43].

Figure 5 summarizes the resulting activities obtained from potentiostatic stepping experiments at 60 °C, measured 30 min after stepping the potential into the range between 0.4 and 0.55 V. As expected, both PtRu-based electrocatalysts show a superior activity as compared to the Pt catalyst on all examined potentials. This better performance of the PtRu catalysts was explained by a bifunctional reaction mechanism for oxidation of CO-containing intermediates, CO_{ads}, on PtRu surfaces. Such mechanism assumes (1) the formation of CO_{ads} species in a methanol dehydrogenation step on Pt sites and (2) the removal of CO_{ads} species via OH adsorbed that are preferentially adsorbed on Ru, formed by dissociative water adsorption. The higher affinity of the Ru surface atoms towards OH formation makes possible the generation of the OH_{ad} required for the oxidation of the CO, which is formed as reaction intermediate during methanol oxidation, with a lower overpotential than on Pt, that is, at almost 0.35 V, instead of potential higher than 0.55 V on

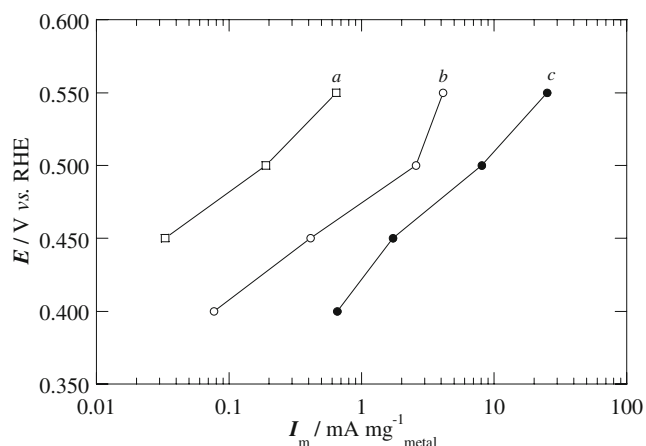


Fig. 5 Electrooxidation of methanol 2.0 mol dm^{-3} on (a) Pt/OMC, (b) Pt₈₀Ru₂₀/OMC, and (c) Pt₈₅Ru₁₅/C catalyzed electrodes at different potentials. Temperature $60 \text{ }^\circ\text{C}$, $0.50 \text{ mol dm}^{-3} \text{ H}_2\text{SO}_4$, $1,800 \text{ s}$ for each potential. Currents were normalized by the total metal content in the electrodes

Pt [44]. This effect leads to the higher activity for the overall methanol oxidation process on PtRu compared to Pt, as shown in Fig. 6.

Comparing the activities of the two PtRu/OMC catalysts, the methanol oxidation activity on Pt₈₅Ru₁₅/OMC is higher than on the Pt₈₀Ru₂₀/OMC catalyst, confirming the results obtained in cyclic voltammetry measurements.

Preliminary test in DMFC

Figure 6 shows the voltage and power density vs. current density curves obtained in the single DMFC operating with a 2 mol dm^{-3} aqueous methanol solution at $60 \text{ }^\circ\text{C}$ and atmospheric pressure. The cathode feed was pure O₂, at atmospheric pressure, to maximize the activity of the cathode and thereby to minimize cathode effects on the relative activities of the cells. It is apparent that there are differences in performance for the different catalysts. The curves show that the open-circuit potential with Pt₈₅Ru₁₅/OMC is 0.131 and 0.107 V higher than those with Pt₈₀Ru₂₀/OMC and Pt₈₅Ru₁₅/Vulcan, respectively. The best performance is obtained when the Pt₈₅Ru₁₅/OMC catalyst is used to prepare the anodes. Then, the performance of the catalysts in the single DMFC follows the order of activity found for the oxidation of methanol in the three-electrode cell experiments; so, in spite of the different conditions, the results of the two types of experiments are consistent. In addition, the difference between the curves is maintained in the whole current interval. This means that the difference is due only to the nature of the catalysts in the anode since Pt/C catalyst with the same loading was coated on the cathode side and depends strongly on the material support. This can be justified by taking into account that prepared Pt₈₅Ru₁₅/OMC and Pt₈₅Ru₁₅/Vulcan catalysts have the

same composition and metal loading, and their mean particles sizes are very similar.

On the other hand, the comparison of the results obtained in single DMFC with published data is not easy because the operational conditions and the MEA composition are not always the same. However, it is possible to establish some comparisons. The performance of MEA (a) in Fig. 6 at the technically interesting potential of 0.4 V was $0.056 \text{ A mg}_{\text{Pt}}^{-1}$. This value is comparable to that reported by other authors for single DMFC working at similar conditions, which used PtRu-supported catalysts synthesized by the FAM. Thus, a DMFC working at $70 \text{ }^\circ\text{C}$ with a Pt₇₅Ru₂₅/Vulcan XC-72[®] anode catalyst showed a mass activity of $0.028 \text{ A mg}_{\text{Pt}}^{-1}$ at 0.4 V [32]. Another kind of comparison can be done using the peak power density given by several MEAs normalized with respect to the anode metal loading. For MEA (a) in Fig. 6, it was equal to $40.5 \text{ mW mg}_{\text{metal}}^{-1}$. This value was higher than those of 25.1 and $28.7 \text{ mW mg}_{\text{metal}}^{-1}$ corresponding to two MEAs, operating at $60 \text{ }^\circ\text{C}$ (2 M , MeOH, dry oxygen) with Pt₇₅Ru₂₅/carbon aerogel and Pt₅₀Ru₅₀/carbon aerogel as anode electrocatalysts, respectively [22].

Conclusion

The work described in this paper presented the use of PtRu/OMC as catalysts in technical electrodes for practical liquid-DMFC. First, it has been demonstrated that it is possible to synthesize PtRu/OMC catalysts with a low particle size and a high degree of dispersion. These catalysts were utilized to manufacture technical electrodes which showed a high activity towards methanol electro-oxidation, as we pointed out in half-cell and single-fuel-cell experiments. In this work, the effect of Pt-to-Ru atomic

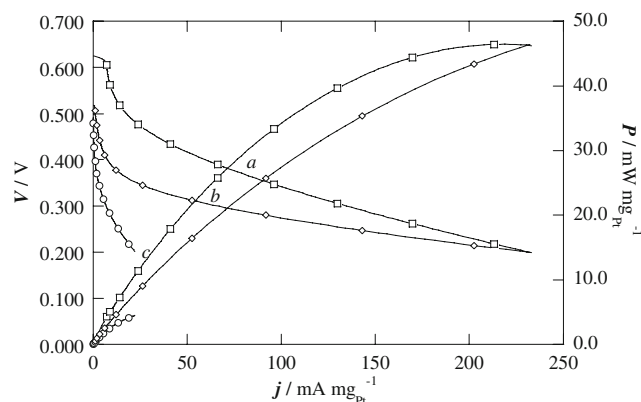


Fig. 6 V - j and P - j polarization curves for liquid-DMFCs with (a) Pt₈₅Ru₁₅/OMC, (b) Pt₈₀Ru₂₀/OMC, and (c) Pt₈₅Ru₁₅/Vulcan catalyzed anodes operating at $60 \text{ }^\circ\text{C}$, $2.0 \text{ mol dm}^{-3} \text{ MeOH}$ at 1.5 mL min^{-1} . Cathode $2.0 \text{ mg}_{\text{Pt}} \text{ cm}^{-2} \text{ Pt/Vulcan}$ catalyst, dry O₂ at 50 mL min^{-1} . Currents normalized per mass of Pt in anodes

ratio on the methanol oxidation under fuel-cell-relevant conditions was investigated too. It can be concluded that the interaction between metals and the OMC support could affect the best Pt-to-Ru atomic ratio for methanol electro-oxidation compared to other PtRu state-of-the-art catalysts, under the same experimental conditions. Finally, OMC open the development of new supported catalysts with controlled bulk composition which can be applied in practical DMFC systems. In this sense, further investigations are required to optimize the structure and physical properties of the OMC, with the purpose of increasing the performance of the DMFC systems in which they are used as catalyst support.

Acknowledgments The authors gratefully acknowledge the financial support given by the Spanish MEC under the project MAT2005-06669-C03-03 (FEDER) and CEGASA.

References

- García BL, Weidner JW (2007) In: White RE, Vayenas CG, Gamboa-Aldeco ME (eds) *Modern aspects of electrochemistry*, vol. 40. Springer, New York
- Gurau B, Smotkin ES (2002) *J Power Sources* 112:339
- Scott K, Shukla AK (2007) In: White RE, Vayenas CG, Gamboa-Aldeco ME (eds) *Modern aspects of electrochemistry*, vol. 40. Springer, New York
- Dicks AL (2006) *J Power Sources* 156:128
- Liu H, Songa C, Zhang L, Zhang J, Wang H, Wilkinson DP (2006) *J Power Sources* 155:95
- Joo JB, Kim P, Kim W, Kim J, Yi J (2006) *Catal Today* 111:171
- Ambrosio EP, Francia C, Gerbaldi C, Penáís N, Spinelli P, Manzoli M, Ghiotti G (2008) *J Appl Electrochem* 38:1019
- Zhao G, He J, Zhang C, Zhou J, Chen X, Wang T (2008) *J Phys Chem C* 112:1028
- Raghuvver V, Manthiram A (2005) *J Electrochem Soc* 152:A1504
- Zeng J, Su F, Lee JY, Zhao XS, Chen J, Jiang X (2007) *J Mater Sci* 42:7191
- Liu S-H, Lu R-F, Huang S-J, Lo A-Y, Chienbc S-H, Liu S-B (2006) *Chem Commun* 32:3435
- Joo SH, Pak C, You DJ, Lee S-A, Lee HI, Kimb JM, Changa H, Seung D (2006) *Electrochim Acta* 52:1618
- Lizcano-Valbuena WH, Caldas de Azevedo D, Gonzalez ER (2004) *Electrochim Acta* 49:1289
- Petrii AO (2008) *J Solid State Electrochem* 12:609
- Liu Y-C, Qiu X-P, Huang Y-Q, Zhu W-T (2002) *J Power Sources* 111:160
- Ding J, Chana K-Y, Rena J, Xiao F-S (2005) *Electrochim Acta* 50:3131
- Ren J, Ding J, Chan K-Y, Wang H (2007) *Chem Mater* 19:2786
- Arbizzani C, Beninati S, Manferrari E, Soavi F, Mastragostino M (2007) *J Power Sources* 172:578
- Lin M-L, Huang C-C, Lo M-Y, Mou C-Y (2008) *J Phys Chem C* 112:867
- Liu S-H, Yu W-Y, Chen C-H, Lo A-Y, Hwang B-J, Chien S-H, Liu S-B (2008) *Chem Mater* 20:1622
- Chai GS, Yoon SB, Kim JH, Yu J-S (2004) *Chem Comm* 23:2766
- Du H, Li B, Kang F, Fu R, Zeng Y (2007) *Carbon* 45:429
- Choi J-S, Chung WS, Ha HY, Lim T-H, Oh I-H, Hong S-A, Lee H-I (2006) *J Power Sources* 156:466
- Lázaro MJ, Calvillo L, Bordejé EG, Moliner R, Juan R, Ruiz CR (2007) *Micropor Mesopor Mater* 103:158
- Gonzalez ER, Ticianelli EA, Pinheiro ALN, Perez J (1997) *Patente Brasileira*, INPI-SP no. 00321
- Chai GS, Yoon SB, Yu JS, Choi JH, Sung YE (2004) *J Phys Chem B* 108:7074
- Antolini E, Passos RR, Ticianelli EA (2002) *Electrochim Acta* 48:263
- Weibel A, Bouchet R, Boule'h F, Knauth P (2005) *Chem Mater* 17:2378
- Mascarenhas YP, Pinheiro JMV (1985) *Programa para Cálculo de Parâmetro de Rede pelo Método de Mínimos Quadrados*. Salvador, SBPC
- Chu D, Gilman S (1996) *J Electrochem Soc* 143:1685
- Salgado JRC, Quintana JJ, Calvillo L, Lázaro MJ, Cabot PL, Esparbé I, Pastor E (2008) *Phys Chem Chem Phys* 10:6796
- Lizcano-Valbuena WH, Paganin VA, Gonzalez ER (2002) *Electrochim Acta* 47:3715
- Antolini E, Salgado JRC, Santos LGRA, Garcia G, Ticianelli EA, Pastor E, Gonzalez ER (2006) *J Appl Electrochem* 36:355
- Iúdice de Souza JP, Iwasita T, Nart FC, Vielstich W (2000) *J Appl Electrochem* 30:43
- Gasteiger HA, Markovic N, Ross PN, Cairns EJ (1994) *J Phys Chem* 98:617
- Schmidt TJ, Noeske M, Gasteiger HA, Behm RJ, Britz P, Brijoux W, Bönemann H (1998) *J Electrochem Soc* 145:925
- Watanabe M, Motoo S (1975) *J Electroanal Chem* 60:267
- Dinh HN, Ren X, Garzon FH, Zelenay P, Gottesfeld S (2000) *J Electroanal Chem* 491:222
- Kawaguchi T, Sugimoto W, Murakami Y, Tasaku Y (2004) *Electrochem Comm* 6:480
- Bock C, McDougall B, LePage Y (2004) *J Electrochem Soc* 158: A1269
- Jiang J, Kucernak A (2003) *J Electroanal Chem* 543:187
- Schmidt TJ, Gasteiger HA, Behm RJ (1999) *J Electrochem Soc* 146:1296
- Sivakumar P, Tricoli V (2006) *Electrochim Acta* 51:1235
- Ruth K, Vogt M, Zuber R (2003) In: Vielstich W, Gasteiger HA, Lamm A (eds) *Handbook of fuel cells—fundamentals, technology and applications*, vol 3. Wiley, Chichester